

State-Selective Differential Cross Section Measurements for the One-Electron Capture Process in C^{3+} -He and C^{3+} -Ne Systems at $E_{\text{lab}} = 33$ eV

Yoh Itoh*

Physics Laboratory, Faculty of Science, Josai University, Saitama 350-0295, Japan

(Received)

Using a crossed-beam apparatus, we measured the relative state-selective differential cross sections (DCSs) for the following reactions: $C^{3+} (1s^2 2s^2 S) + He (1s^2 ^1S) \rightarrow C^{2+} (1s^2 2s2p ^1P) + He^+ (1s ^2S) + 10.6$ eV and $C^{3+} (1s^2 2s^2 S) + Ne (2p^6 ^1S) \rightarrow C^{2+} (1s^2 2p^2 ^1D) + Ne^+ (2p^5 ^2P) + 8.2$ eV. The scattering angle studied in the laboratory frame, θ_{lab} , was from -3.0° to 24° , and the laboratory collision energy E_{lab} was 33 eV. In both systems, the DCSs for the reaction are zero at the center-of-mass angle $\theta_{\text{cm}} = 0$, and show a peak at a certain angle and a broad hump at larger angles. A classical trajectory analysis within the two-state approximation based on the ab initio potentials for $(CHe)^{3+}$ revealed that these structures observed are ascribed to the reactions that occur in different trajectories. The peak corresponds to the reactions occurring in the outgoing part of the trajectory, and the hump is associated with the reactions occurring mainly in the incoming part of the trajectory.

1. Introduction

State-selective differential cross section (DCS) measurement for the one-electron capture process of the type: $A^{q+} + B \rightarrow A^{(q-1)+} + B^+ + \Delta E$, where q denotes the charge-state of projectile ions, and ΔE stands for the exothermicity, is a powerful means for understanding the collision mechanism as well as obtaining information about the interaction potentials. For instance, we have recently measured¹⁾ the state-selective DCSs for the one-electron capture process in N^{5+} and O^{5+} on He collisions below the collision energy in the laboratory frame, $E_{\text{lab}} = 50$ eV, and analyzed the results using ab initio potentials. Although Ishii et al. reported that the integral cross sections were almost the same,²⁾ we found that the collision

mechanisms were much different; i.e., the DCS was very large at the center-of-mass angle $\theta_{\text{cm}} = 0$ in the N^{5+} -He system, whereas it was completely zero in the O^{5+} -He system. Because the interaction potentials corresponding to the reaction in the O^{5+} -He system are all repulsive in character,³⁾ the scattering angles are always positive; thus, the DCS at $\theta_{\text{cm}} = 0$ becomes zero. On the other hand, the ab initio potential for $(\text{NHe})^{5+}$ shows a shallow well in the initial channel.⁴⁾ A classical trajectory analysis based on the ab initio potentials revealed that the scattering angle became zero owing to the cancellation of the deflections due to the attractive and repulsive forces. Therefore, we attributed the peak that appears at $\theta_{\text{cm}} = 0$ to the forward glory effect.¹⁾ We also observed the glory scattering in the Ne^{4+} -He system.⁵⁾ Thus, we experimentally demonstrated that when the attractive force is sufficiently strong, the glory scattering is a very common phenomenon in the one-electron capture process.

In this paper, we report on the measured DCSs for the one-electron capture process, as well as for the elastic scattering, in the C^{3+} with He and with Ne collisions. One of our interests was to study the change in the DCSs for the reaction due to the different long-range attractive forces produced by the different dipole polarizabilities of the targets.

Absolute integral cross sections for the one-electron capture process in the C^{3+} -He were measured by Ishii et al.,²⁾ and the state selectivity of the reaction was measured by Kimura et al.⁶⁾ at $E_{\text{lab}} = 3$ keV and by Lennon et al.⁷⁾ at $E_{\text{lab}} = 3$ –15 keV. Wu et al.⁸⁾ reported theoretical integral cross sections on the basis of the ab initio potentials using the quantum-mechanical molecular-orbital close-coupling method. Measured results for the C^{3+} -Ne system in the energy regions comparable to that of the present measurements were scarce. Lee et al.⁹⁾ reported the final state analysis of the reactions at $E_{\text{lab}} = 6$ keV. To the best of our knowledge, no DCSs for the elastic scattering and one-electron transfer reaction were reported for the

systems reported in this study.

2. Experimental Procedure

The experimental procedure was reported previously.¹⁾ In brief, we produced $^{13}\text{C}^{3+}$ ions with an electron beam ion source (EBIS) using $^{13}\text{C}^{16}\text{O}$ as the source gas to eliminate impurity ions with the same mass-to-charge ratio, $m/q = 4$, for example, $^{12}\text{C}^{3+}$ and $^{16}\text{O}^{4+}$. Energy- and momentum-selected ions were crossed with a supersonic target beam, and the energies of the scattered ions were analyzed using an electrostatic analyzer with a position-sensitive detection system.

The angular distribution was measured from the energy spectrum that was obtained by rotating the detector in 0.3° steps in the laboratory frame. The scattering angle studied in the laboratory frame, θ_{lab} , was from -3.0° to 24° . The accumulation time was approximately 2.0 h at each angle. A peak-fitting program was used to integrate the ion counts under the peak area. The measured signals were then converted to the relative DCS in the center-of-mass system in a standard manner. In this study, the DCS measured is proportional to $d\sigma/d\Omega$, not to $d\sigma/d\theta_{\text{cm}} = 2\pi \sin\theta_{\text{cm}} d\sigma/d\Omega_\theta$, where $d\Omega_\theta = 2\pi \sin\theta_{\text{cm}} d\theta_{\text{cm}}$ is the element of the solid angle for the polar direction θ_{cm} . The same detection efficiency for the elastically scattered C^{3+} ions and for the C^{2+} ions produced by the reactions was assumed in the determination of DCSs for each channel.

Accurate collision energy determination is essential for identifying reaction channels from the ion energy spectrum. Therefore, we simultaneously measured the elastically scattered ions in the $\text{C}^{3+}\text{-He}$ system and compared their angular dependences with the calculated ones, changing the collision energy as a parameter to reproduce the measured

results. The collision energy of the present measurements was determined to be $E_{\text{lab}} = 33 \pm 1$ eV.

In the $\text{C}^{3+}\text{-Ne}$ system, the energy of the elastically scattered ions depends less on the scattering angle as compared with the case of He as the target, because the projectile C^{3+} is lighter than the target. Therefore, we used He gas to determine collision energy before we start the measurements.

The overall angular resolution in the laboratory frame was approximately $\pm 0.8^\circ$ at the full width at half maximum. This corresponds to approximately ± 0.05 rad at $\theta_{\text{cm}} = 0.35$ rad for the $\text{C}^{3+}\text{-He}$ system, and ± 0.02 rad at $\theta_{\text{cm}} = 0.15$ rad in the $\text{C}^{3+}\text{-Ne}$ system.

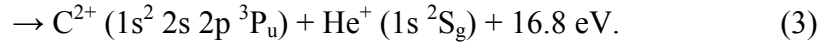
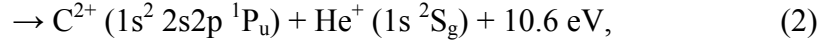
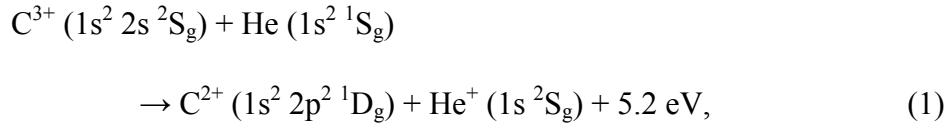
We observed the C^{2+} ions at an angle of approximately $\theta_{\text{lab}} = 0^\circ$ even when the target beam was not being used. Therefore, we carefully measured the background counts and thus determined the true signal counts. In the present collision systems, all the C^{2+} ions observed at approximately $\theta_{\text{lab}} = 0^\circ$ were determined to be noise signals.

3. Results

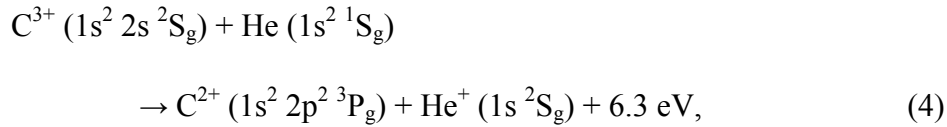
3.1 Final-state analysis in $\text{C}^{3+}\text{-He}$

Figure 1(a) shows the measured energy spectra obtained from $\theta_{\text{lab}} = 3.0^\circ\text{-}24^\circ$ in a density plot, i.e., the energy spectra measured at different angles are plotted in the two-dimensional graph, and the intensities of the scattered ions are indicated by the darkness of the color. Examples of the individual spectra obtained at $\theta_{\text{lab}} = 4.5^\circ$ and 10.5° are shown in Figs. 1(b) and 1(c), respectively. The calculated positions for the elastically scattered C^{3+} ions at $E_{\text{lab}} = 33$ eV, which corresponds to the center-of-mass energy $E_{\text{cm}} = 7.8$ eV, are indicated by a curve labeled E in Fig. 1(a). The energy positions of the scattered ions corresponding to

the following reaction channels are shown by the curves labeled 1, 2, and 3, respectively:



The radial coupling is considered to be responsible for the electron capture mechanism at low energies;¹⁰⁾ hence, the symmetry of the quasi-molecular states generated from the initial states and the final states is conserved. The parity symbols gerade (g) and ungerade (u) were indicated in these equations to examine the quasi-molecular states. The quasi-molecular state generated from $\text{C}^{3+} (1s^2 2s^2 S_g)$ and $\text{He} (1s^2 {}^1S_g)$ is ${}^2\Sigma^+$; therefore, here, we only considered the final channels that have the symmetry of ${}^2\Sigma^+$. The following reaction channel is not considered here:



because the symmetries of the quasi-molecular states generated from P_g and S_g states are Σ^- and Π .¹¹⁾ We found reaction channel (2) to be the dominant process in this energy region, i.e., the electron capture to the excited state of the C^{2+} . This agrees well with the measured results reported previously. For example, Kimura et al.⁶⁾ demonstrated that all the channels shown above, as well as for the reaction producing $\text{C}^{2+} (1s^2 2s^2 {}^1S_g) + \text{He}^+ (1s^2 S_g) + 23.3 \text{ eV}$, were opened at the collision energy E_{lab} of 3 keV. Of these reaction channels, reaction channel (2) was found to be the most dominant. Similar results were reported by Lennon et al.⁷⁾ at $E_{\text{lab}} = 3\text{--}15 \text{ keV}$. Wu et al.⁸⁾ reported theoretical results on the basis of the ab initio potentials, using the quantum-mechanical molecular-orbital close-coupling method. They also demonstrated

that reaction channel (2) was dominant below $E_{\text{lab}} = 60$ eV; thus, our result supports their conclusion.

3.2 Final-state analysis in $C^{3+}-Ne$

Figure 2 shows an example of the energy spectrum obtained at $\theta_{\text{lab}} = 4.5^\circ$. The collision energy E_{lab} was 33 eV ($E_{\text{cm}} = 20$ eV). The energy positions for the following reaction channels are indicated:

$$C^{3+} (1s^2 2s^2 S_g) + Ne (2p^6 {}^1S_g)$$

$$\rightarrow C^{2+} (1s^2 2p^2 {}^1S_g) + Ne^+ (2p^5 {}^2P_u) + 3.7 \text{ eV}, \quad (5)$$

$$\rightarrow C^{2+} (1s^2 2p^2 {}^1D_g) + Ne^+ (2p^5 {}^2P_u) + 8.2 \text{ eV}, \quad (6)$$

$$\rightarrow C^{2+} (1s^2 2p^2 {}^3P_g) + Ne^+ (2p^5 {}^2P_u) + 9.3 \text{ eV}, \quad (7)$$

$$\rightarrow C^{2+} (1s^2 2s 2p {}^1P_u) + Ne^+ (2p^5 {}^2P_u) + 13.6 \text{ eV}. \quad (8)$$

The symmetry of the quasi-molecular state generated from the initial channel is again ${}^2\Sigma^+$. Reaction channel (7) to the $C^{2+} (1s^2 2p^2 {}^3P_g)$ was not considered in the case of the He target. While in the case of the Ne target, the electronic state of the product Ne^+ is 2P_u ; therefore, the ${}^2\Sigma^+$ state is generated from this configuration;¹¹⁾ thus this channel can in principle contribute to the reaction.

Although the energy resolution of the present measurement is insufficient to separate reaction channels (6) and (7), the peak position coincides with the energy position for reaction channel (6). The reactions in these channels are often called transfer excitation; i.e., the electron capture and the electronic excitation of projectile ions occur at the same time; this is a typical two-electron process. This type of reaction is also called the core-varying single-electron capture¹²⁾ or type II reaction.¹³⁾

To the best of our knowledge, the final-state analysis of the one-electron capture process in C^{3+} -Ne was reported only by Lee et al.⁹⁾ at $E_{\text{lab}} = 6$ keV. They reported that reaction channel (8), i.e., the simple electron capture process to the excited state of C^{2+} , was the most prominent, and the second dominant process was reaction channel (6), the transfer excitation. The importance of the transfer excitation was often reported to increase with decreasing in collision energy.^{14, 15)} The present result seems to agree well with this collision energy dependence.

3.3 DCSs measured in C^{3+} -He and C^{3+} -Ne systems

Figure 3 shows relative DCSs in the center-of-mass system for reaction channel (2) in the C^{3+} -He system as well as for the elastic scattering. Because we performed relative DCS measurements, the peak intensity for the reaction has been normalized to unity. The error bars show the sum of the fluctuations of the ion signal and the imprecision of the peak-fitting procedure. The features of the DCSs for the reaction are as follows: (i) it is zero at the scattering angle of approximately $\theta_{\text{cm}} = 0$ rad, (ii) the DCS shows a prominent peak at $\theta_{\text{cm}} = 0.27$ rad, and (iii) it shows a broad hump at approximately $\theta_{\text{cm}} = 0.6$ rad. The DCSs for the elastic scattering show almost no structure and decrease monotonically with increasing scattering angle.

Figure 4 shows the relative DCSs for both the elastic and inelastic scatterings in the C^{3+} -Ne system. Note that the DCS for the elastic scattering is divided by 10 in order to show the data on a comparable scale. Channel (6) was analyzed to be the main reaction channel. The DCS for the reaction is again zero at approximately $\theta_{\text{cm}} = 0$ rad and shows a peak at $\theta_{\text{cm}} = 0.07$ rad; then, it decreases almost monotonically. The hump seen in the case of the C^{3+} -He

system was not clearly observed. The feature of the DCSs for the elastic scattering is nearly the same as that in the C^{3+} -He system.

4. Discussion

4.1 Final-state analysis based on the reaction window

For a semiquantitative understanding of the state selectivity observed in the present collision systems, we compared the measured exothermicity with the peak position of the calculated reaction windows. We found experimentally that only few reaction channels were opened; hence, we can safely assume that we will apply the two-state approximation in the following analysis.

The reaction window based on the Landau-Zener formula¹⁶⁾ and that based on the extended version of the classical over barrier (ECOB) model¹⁷⁾ were examined. Atomic units are used hereafter unless otherwise indicated.

Zhu and Nakamura¹⁸⁾ have reported the accurate formulas for the calculation of the Landau-Zener transition probability. To apply these formulas to the present analysis, however, we have no accurate information on the interaction potentials especially for the C^{3+} -Ne system. Therefore, the conventional method of calculation¹⁶⁾ was performed in this work to compare the state selectivity of the systems under the same conditions.

The coupling matrix elements H_{12} were evaluated by applying the empirical formula proposed by Kimura et al.,¹⁹⁾ i.e.,

$$H_{12} = (5.48 / \sqrt{q}) \exp(-1.324\alpha R_c / \sqrt{q}), \quad (9)$$

where $R_c = (q - 1) / \Delta E$ is the crossing radius of the interaction potentials and $\alpha = \sqrt{2I_t}$ where I_t is the ionization energy of the target. Equation (9) was used for both the C^{3+} -He and

C^{3+} -Ne systems.

The exothermicity for the one-electron transfer reaction based on the ECOB model was obtained as $(q - 1) / R_{cd}$, where $R_{cd} = (2\sqrt{q} + 1) / I_i$ is the capture distance at which the reaction can occur. The width of the reaction window was calculated using Eq. (20) in Ref. 17.

The calculated reaction windows under both models for the collision energy E_{lab} of 33 eV are shown in Fig. 5. The peak value of the reaction window was normalized to unity. The measured exothermicity observed in the C^{3+} -He collision is close to the maximum of the reaction window based on the Landau-Zener model, whereas for the C^{3+} -Ne system, the ECOB model seems to reproduce the experimental results. At the low collision energies, the choice of the coupling matrix element H_{12} affects the calculated reaction windows. We cannot conclude at present which model is most suitable for analyzing the state selectivity in the present collision systems. The reaction window calculations at least suggest that the reaction channel with the smaller exothermicity is more favored in the C^{3+} -Ne system than in the C^{3+} -He system, and this trend agrees with the measured results.

4.2 Classical trajectory analysis in C^{3+} -He

To determine the origin of the features observed in the DCSs for the one-electron transfer reaction, we applied the classical trajectory analysis within the two-state approximation. We referred to the theoretical potentials reported by Wu et al.,⁸⁾ then set up a Morse-type potential for the initial channel:

$$V_{in}(r) = 0.015 \left\{ \exp[1.098(5.410 - r)] - 2 \exp[0.549(5.410 - r)] \right\}. \quad (10)$$

Only the Coulomb repulsive potential and the exothermicity were considered for the reaction

channel:

$$V_{\text{out}}(r) = 2/r - 0.3899. \quad (11)$$

These model and theoretical potentials are compared in Fig. 6.

We also evaluated that the energy difference of the theoretical potentials is 0.017 at the avoided crossing at $r = 5.2$; then, we determined H_{12} to be 0.00865, which is one-half of the energy difference at the crossing point.¹⁹⁾ This value is approximately twofold smaller than that obtained from Eq. (9).

Applying these model potentials, we first calculated the deflection function, i.e., the deflection angle Θ as a function of the impact parameter b . Generally, the scattering angle in the center-of-mass system is given by $\theta_{\text{cm}} = |\Theta|$. The upper half of the curve in Fig. 7 corresponds to the deflection function when the reaction occurs in the incoming part of the trajectory. In this reaction path, the Coulomb repulsion force primarily determines the trajectory; thus, the deflection angle is always positive. The lower part of the curve in Fig. 7 corresponds to the deflection function when the reaction occurs in the outgoing part of the trajectory. The deflection function is again found to be always positive; this means that the attractive part of the interaction potential is weak. These trends of the deflection function explain the reason why the DCS for the reaction is completely zero at approximately $\theta_{\text{cm}} = 0$.

The classical DCSs for the reaction were calculated using the following well-known formula:

$$\frac{d\sigma}{d\Omega} = \sum_j \frac{b_j}{\sin \theta_{\text{cm}}} \left| \frac{d\Theta}{db_j} \right|^{-1} \cdot P(b_j), \quad (12)$$

where b_j is the possible impact parameter that will result in the same scattering angle θ_{cm} in the center-of-mass system, and $P(b_j)$ is the transition probability. The conventional Landau–

Zener formula¹⁶⁾ was used again to estimate $P(b_j)$ for the analysis. The quantities of H_{12} and R_c evaluated from the ab initio potentials were adopted. The calculated DCSs are shown in Fig. 8. Two components that reflect the different trajectories are shown separately. The measured DCSs were fitted to the calculated ones at approximately $\theta_{cm} = 0.6$ rad. A good agreement between the calculated DCSs and the measured results was achieved.

The component of the DCS that corresponds to the electron capture that occurs in the outgoing part of the trajectory increases steeply at $\theta_{cm} = 0.27$ rad, and decreases monotonically with increasing scattering angles. This sudden increase in the DCS is due to the divergence of the classical DCS when $d\Theta/db$ becomes zero. Olson and Kimura²⁰⁾ referred to this peak as “inelastic rainbow” analogous to the rainbow phenomenon in elastic collisions. On the other hand, the DCS component that corresponds to the reaction that occurs in the incoming part of the trajectory appears to increase at $\theta_{cm} = 0.48$ rad shows a peak at $\theta_{cm} = 0.67$ rad and then decreases monotonically.

We see in Fig. 8 that (i) the measured peak of the DCS can be well reproduced by the inelastic rainbow peak and (ii) the hump is constructed primarily by the reaction that occurs in the incoming part of the trajectory. Thus, we conclude that the structures in the measured DCS correspond to the reaction caused by the different trajectories.

4.3 Comparison of the DCSs in the reduced impact parameter

The ab initio potentials for $(CNe)^{3+}$ have not been reported up to now; therefore, the detailed analysis described in the previous subsection is not possible for the C^{3+} -Ne system. For qualitatively understanding the feature of the DCS in the C^{3+} -Ne system, the measured DCSs for the reaction in the C^{3+} -He and C^{3+} -Ne systems are compared in Figs. 9(a) and 9(b),

respectively. The reduced scattering angle $E_{\text{cm}} \theta_{\text{cm}}$ that correlates with the impact parameter²¹⁾ was used for the comparison.

The overall angular dependence of the DCS for the reaction in the $\text{C}^{3+}\text{-Ne}$ system appears to be similar to that for the reaction in the $\text{C}^{3+}\text{-He}$; hence, the peak of the DCS could be attributed to the inelastic rainbow. As seen in Fig. 9(b), the peak shifts to smaller scattering angles in comparison with the case of $\text{C}^{3+}\text{-He}$. We also compared the reduced cross sections, i.e., $\theta_{\text{cm}} \sin \theta_{\text{cm}} d\sigma / d\Omega$, for both systems as a function of the reduced scattering angle. In this comparison, the same trend of the peak shift was detected although the peak structure was strongly depressed by the factor $\theta_{\text{cm}} \sin \theta_{\text{cm}}$.

The inelastic rainbow correlates with the reaction that occurs in the outgoing part of the trajectory; hence, the trajectory is strongly affected by the attractive part of the interaction potential, and the strong attractive force naturally causes the peak position to be at smaller scattering angles. A candidate that causes the peak shift is the long-range attractive force due to the large polarizability coefficient of the Ne target. The polarization potential is expressed as $V(r) = -q^2 \alpha_{\text{D}} / 2r^4$, where α_{D} denotes the dipole polarizability, that is, 1.384 a.u. for He and 2.670 a.u. for Ne.²²⁾ Therefore, the polarization force is approximately two times stronger in the $\text{C}^{3+}\text{-Ne}$ system than in the $\text{C}^{3+}\text{-He}$ system. However, the attractive force is found to be insufficient to result in the glory scattering measured, for example, in the N^{5+} and $\text{Ne}^{4+}\text{-He}$ collisions.^{1,5)}

The hump observed in the $\text{C}^{3+}\text{-He}$ system was not clearly observed in the case of the $\text{C}^{3+}\text{-Ne}$ collisions. The reason for this is unclear at present because of the lack of accurate interaction potentials. One possible explanation is that this trend is caused by the impact parameter dependence of the transition probability. In the previous subsection, we concluded

that the hump was due to the reaction that occurs in the incoming part of the trajectory. The onset of the hump correlates with the collisions with the impact parameters that are slightly smaller than the crossing radius. In the Landau–Zener approximation, the magnitude of the transition probability depends much on such conditions. If the transition probabilities are small for these impact parameters, the reaction that occurs in the incoming part of the trajectory contributes less to the total DCS for the reaction. Consequently, the DCS after the peak at a certain angle will show less structure.

To support the discussion above, the reaction probabilities $P(\theta_{\text{cm}})$ were estimated from the DCSs measured for the elastic scattering and for the reaction. Here, the reaction probability is defined as the ratio of the inelastic DCS to the sum of the elastic and inelastic DCSs at the same scattering angle θ_{cm} . The results are shown in Fig. 10. The reduced scattering angle is again used for the comparison. Note that we were unable to evaluate $P(\theta_{\text{cm}})$ in the C^{3+} –Ne system below $E_{\text{cm}} \theta_{\text{cm}} = 1.5$ eV rad, because of the lack of elastic DCSs. The reaction probability in the C^{3+} –He system begins to increase steeply at approximately $E_{\text{cm}} \theta_{\text{cm}} = 1.5$ eV rad, and it shows structures that correspond to the inelastic rainbow and the broad hump observed in the DCS for the reaction. On the other hand, in the C^{3+} –Ne system, the reaction probability appears to increase at nearly the same $E_{\text{cm}} \theta_{\text{cm}}$ for the He target case, but increases rather monotonically and shows less structure than that in the C^{3+} –He system. The smaller $E_{\text{cm}} \theta_{\text{cm}}$ naturally corresponds to the scattering with the larger impact parameter. Therefore, as presumed above, the transition probability $P(b)$ in the C^{3+} –Ne system is considered to be small when the impact parameter is slightly smaller than the crossing radius; hence, the DCS for the reaction shows less structure than that in the C^{3+} –He system. Detailed theoretical analyses based on the ab initio potentials will further clarify the difference in these

systems.

5. Summary

We measured the state-selective DCSs in the C^{3+} -He and C^{3+} -Ne systems at $E_{\text{lab}} = 33$ eV. The reaction to the excited state, $C^{2+} (1s^2 2s2p \ ^1P)$, has been found to be dominant in the C^{3+} -He collisions. On the other hand, only the transfer excitation to the $C^{2+} (1s^2 2p^2 \ ^1D)$ state has been observed in the C^{3+} -Ne system. We analyzed the distributions of the final channels on the basis of the reaction window calculations applying the Landau-Zener model and the ECOB model. Both models revealed that the reaction with smaller exothermicity was more favored in the C^{3+} -Ne system than in the C^{3+} -He system. The classical trajectory calculation based on the ab initio potentials for the C^{3+} -He collisions could reproduce the trends of the measured DCS for the reaction. Thus, the measured peak in the DCS was concluded to be due to the inelastic rainbow, and the hump was produced mainly by the contribution of the reaction that occurs in the incoming part of the trajectory. The shift of the peak to smaller angles in the C^{3+} -Ne system was temporarily assigned to the effect of the strong attractive forces caused by the larger polarizability of the Ne target.

Acknowledgements This paper is dedicated to the late Dr. Kazumasa Ohtsuki, who provided me with his unpublished theoretical potentials. This work was partly supported by a Grant-in-Aid for Scientific Research (17540373).

* yitoh @josai.ac.jp

References

- 1) Y. Itoh, J. Phys. B **44**, 175202 (2011) [Erratum **44**, 239601 (2011)].
- 2) K. Ishii, A. Itoh, and K. Okuno, Phys. Rev. A **70**, 042716 (2004).
- 3) N. Shimakura, S. Yamada, S. Suzuki, and M. Kimura, Phys. Rev. A **51**, 2989 (1995).
- 4) M. C. Bacchus-Montabonel, Phys. Rev. A **36**, 1994 (1987).
- 5) Y. Itoh, J. Phys. Soc. Jpn. **83**, 075001 (2014).
- 6) M. Kimura, T. Iwai, Y. Kaneko, N. Kobayashi, A. Matsumoto, S. Ohtani, K. Okuno, S. Takagi, H. Tawara, and S. Tsurubuchi, J. Phys. B **15**, L851 (1982).
- 7) M. Lennon, R. W. McCullough, and H. B. Gilbody, J. Phys. B **16**, 2191 (1983).
- 8) Y. Wu, Y. Y. Qi, J. Yan, J. G. Wang, Y. Li, R. J. Buenker, D. Kato, and P. S. Krstic, Phys. Rev. A **80**, 022715 (2009).
- 9) A. R. Lee, A. C. R. Wilkins, C. S. Enos, and A. G. Brenton, Int. J. Mass Spectrom. Ion Processes. **130**, 83 (1994).
- 10) M. Gargaud, J. Hanssen, R. McCarroll, and P. Valiron, J. Phys. B **14**, 2259 (1981).
- 11) G. Herzberg: *Molecular Spectra and Molecular Structure. Vol. I: Spectra of Diatomic Molecules* (Van Nostrand Reinhold, New York, 1950) 2nd ed., Chap. VI, p. 318.
- 12) J. Schweinzer and H. Winter, J. Phys. B **23**, 3899 (1990).
- 13) S. E. Butler and A. Dalgarno, Astrophys. J. **241**, 838 (1980).
- 14) B. A. Huber and H-J. Kahlert, J. Phys. B **17**, L69 (1984).
- 15) E. Y. Kamber, K. Akgüngör, C. Leather, and A. G. Brenton, Phys. Rev. A **54**, 1452 (1996).
- 16) K. Taulbjerg, J. Phys. B **19**, L367 (1986).
- 17) A. Niehaus, J. Phys. B **19**, 2925 (1986).

- 18) C. Zhu and H. Nakamura, *J. Chem. Phys.* **102**, 7448 (1995).
- 19) M. Kimura, T. Iwai, Y. Kaneko, N. Kobayashi, A. Matsumoto, S. Ohtani, K. Okuno, S. Takagi, and H. Tawara, *J. Phys. Soc. Jpn.* **53**, 2224 (1984).
- 20) R. E. Olson and M. Kimura, *J. Phys. B* **15**, 4231 (1982).
- 21) F. T. Smith, R. P. Marchi, and K. G. Dedrick, *Phys. Rev.* **150**, 79 (1966).
- 22) P. Schwerdtfeger, <http://ctcp.massey.ac.nz/dipole-polarizabilities>.

Figures

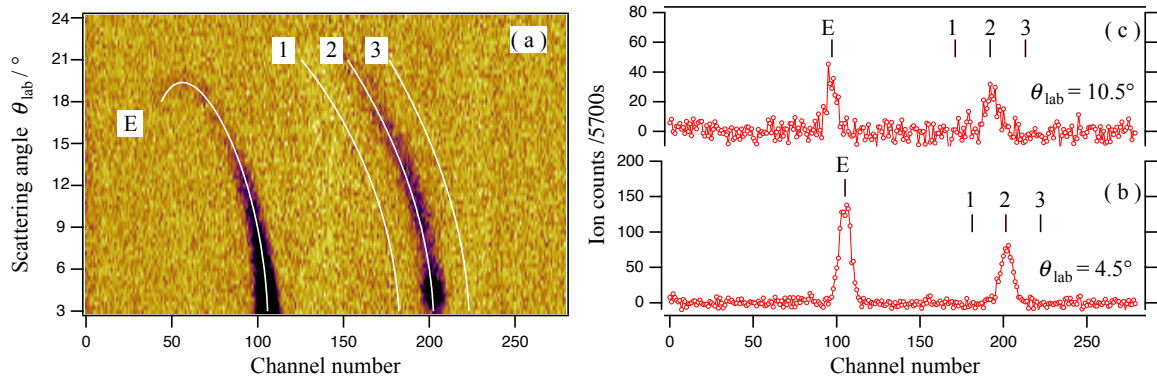


Fig. 1. (Color online) (a) Energy spectra of the scattered ions in the C^{3+} –He system at $E_{\text{lab}} = 33$ eV. Measured spectra are shown in a density plot as a function of scattering angle. The channel number corresponds to the kinetic energy of the ions; the increment of energy is approximately $0.103q$ eV. Curve E: calculated position for the elastically scattered ions. Curves 1, 2, and 3: calculated positions for the one-electron capture signals to the final states, $\text{C}^{2+} (2p^2 \ ^1D)$, $\text{C}^{2+} (2s2p \ ^1P)$, and $\text{C}^{2+} (2s2p \ ^3P)$, respectively. Individual energy spectrum obtained at $\theta_{\text{lab}} = 4.5^\circ$ (b), and at $\theta_{\text{lab}} = 10.5^\circ$ (c).

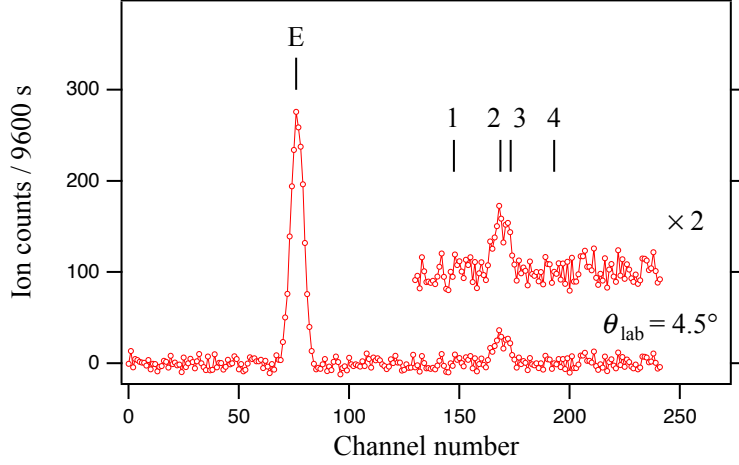


Fig. 2. (Color online) Energy spectrum of the scattered ions in the C^{3+} -Ne system at $E_{\text{lab}} = 33$ eV and $\theta_{\text{lab}} = 4.5^\circ$. The peak labeled E corresponds to the elastic scattering. The energy positions for the reaction channels $C^{2+}(2p^2\ ^1S)$, $C^{2+}(2p^2\ ^1D)$, $C^{2+}(2p^2\ ^3P)$, and $C^{2+}(2s2p\ ^1P)$ are shown by the lines labeled 1, 2, 3, and 4, respectively.

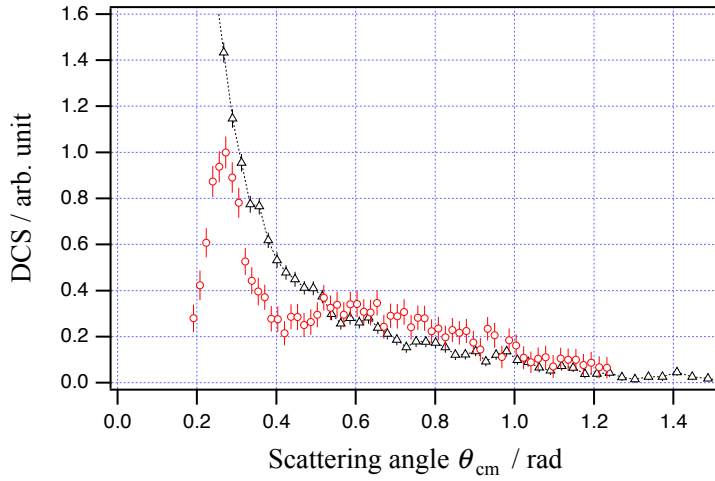


Fig. 3. (Color online) Relative DCSs in the center-of-mass system in the C^{3+} -He collisions at $E_{\text{cm}} = 7.8$ eV; Δ for the elastic scattering, and \circ for the reaction $C^{3+}(1s^2\ 2s\ ^2S) \rightarrow C^{2+}(1s^2\ 2s2p\ ^1P) + He^+(1s\ ^2S) + 10.6$ eV.

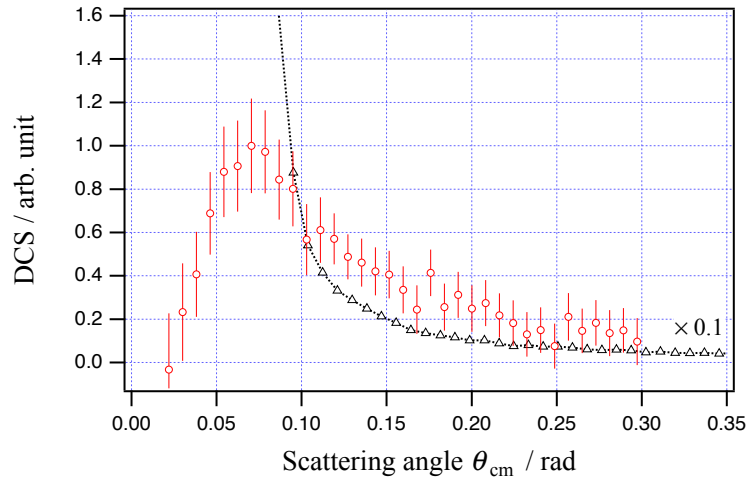


Fig. 4. (Color online) Relative DCSs in the center-of-mass system in the C^{3+} -Ne collisions at $E_{\text{cm}} = 20$ eV; Δ for the elastic scattering and \circ for the reaction $C^{3+} (1s^2 2s^2 S) + \text{Ne} (2p^6 {}^1S) \rightarrow C^{2+} (1s^2 2p^2 {}^1D) + \text{Ne}^+ (2p^5 {}^2P) + 8.2$ eV. The DCS for the elastic scattering is divided by 10.

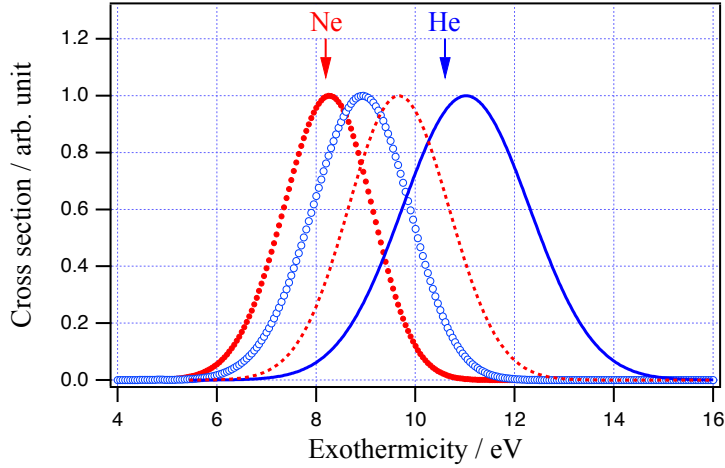


Fig. 5. (Color online) Reaction windows based on the Landau–Zener model at $E_{\text{lab}} = 33$ eV; \circ (blue) for the C^{3+} –He system, and \bullet (red) for the C^{3+} –Ne system. Reaction windows based on the ECOB model at $E_{\text{lab}} = 33$ eV; solid curved line (blue) for the C^{3+} –He system and dashed curve (red) for the C^{3+} –Ne system. The arrow labeled He shows the observed exothermicity in the C^{3+} –He system, and the one labeled Ne indicates that in the C^{3+} –Ne system.

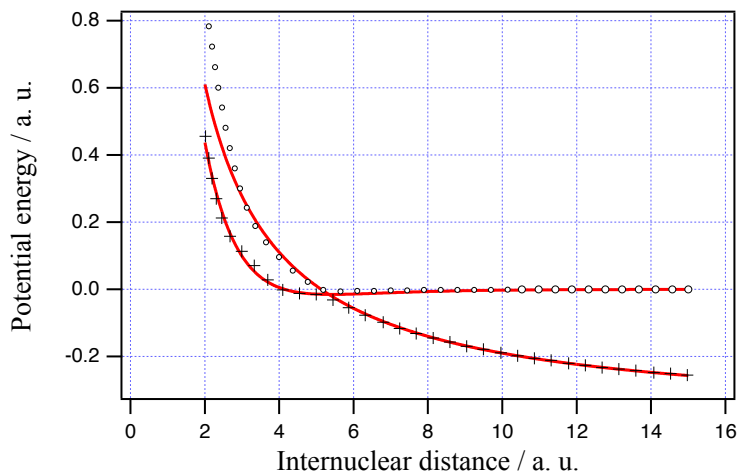


Fig. 6. (Color online) Curves: model potentials used to calculate the DCS in the C^{3+} –He system. \circ , $+$: ab initio potential energies reported by Wu et al.⁸⁾

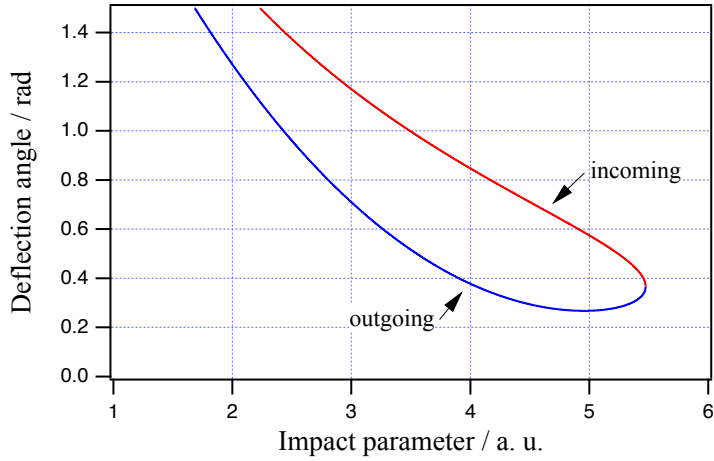


Fig. 7. (Color online) Deflection function for the one-electron capture reaction in the C^{3+} -He system at $E_{\text{lab}} = 33$ eV ($E_{\text{cm}} = 7.8$ eV). The upper part of the curve corresponds to the reaction that occurs in the incoming part of the trajectory, and the lower half of the curve corresponds to the reaction that occurs in the outgoing part of the trajectory.

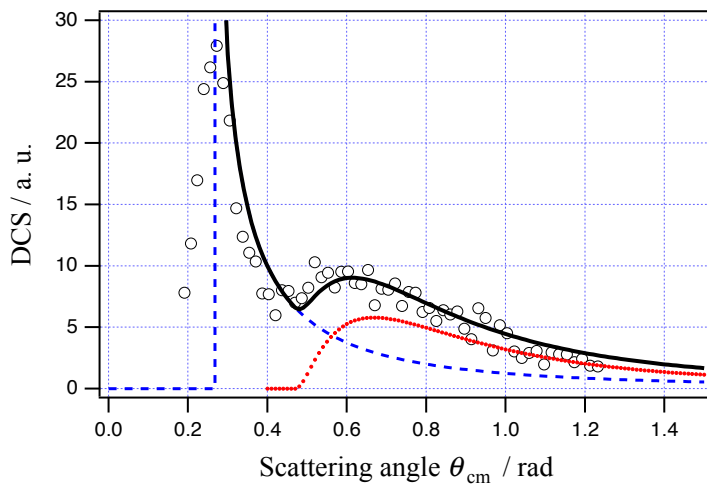


Fig. 8. (Color online) Comparison of the measured and calculated DCSs for the reaction; \circ : measured DCSs. Full curved line: calculated DCSs. Dashed curve: DCS corresponding to the reaction that occurs in the outgoing part of the trajectory. Dotted curve: DCS due to the incoming part of the trajectory.

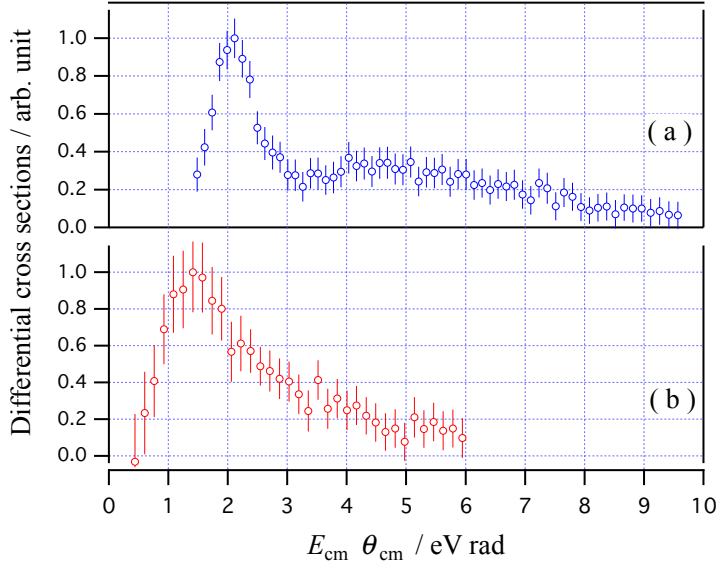


Fig. 9. (Color online) Comparison of the DCSs for the reactions (a) in the C^{3+} –He system and (b) in the C^{3+} –Ne system, in the reduced scattering angle $E_{\text{cm}} \theta_{\text{cm}}$.

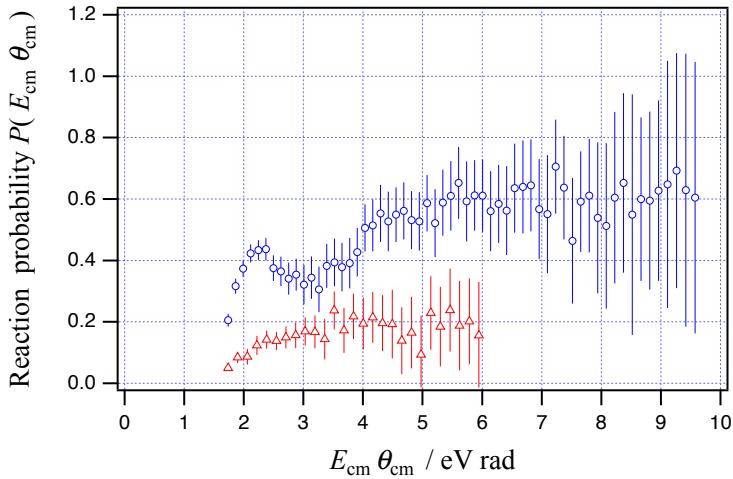


Fig. 10. (Color online) Comparison of the reaction probabilities (see text) in the reduced scattering angle $E_{\text{cm}} \theta_{\text{cm}}$; \circ for the C^{3+} –He system, and Δ for the C^{3+} –Ne system.